Applied Catalysis B: Environmental 323 (2023) 122184

Contents lists available at ScienceDirect

Applied Catalysis B: Environmental

journal homepage: www.elsevier.com/locate/apcatb

Study of the kinetics, mechanisms and catalysis activity of photo-electro degradation of organic pollutants via new neural network based methodology

Han Yu [a,b,f], Zhenzong Zhang [a,*], Sihui Zhan [a], Shuyan Song [c], Shengmin Sun [d], Hui Zhang [e], Linus Zhang [f], Hongbing Yu [a,b,**]

[a] College of Environmental Science and Engineering, Nankai University, Tianjin 300350, PR China
[b] Shenzhen Research Institute, Nankai University, Shenzhen 518000, PR China
[c] State Key Laboratory of Rare Earth Resource Utilization, Changchun Institute of Applied Chemistry, Chinese Academy of Sciences, 5625 Renmin Street, Changchun 130022, PR China
[d] College of Food Engineering, Harbin University of Commerce, Harbin, Heilongjiang 150076, PR China
[e] Key Laboratory of Engineering Dielectrics and Its Application of Ministry of Education & School of Material Science and Engineering, Harbin University of Science and Technology, Harbin 150080, PR China
[f] Division of Water Resources Engineering, Lund University, Lund 22100, Sweden

ARTICLE INFO

Keywords:
Photo-electro treatment
Organics degradation
Modeling
Grey relation analysis
Principal component analysis

ABSTRACT

A novel calculation methodology containing modeling and statistics was developed to assist the experimental process for the investigation of organics treatment process. A continuous-flow photo-electro treatment of Norfloxacin (NOR) was chosen as a target subject. The methodology is based on a new synergistic work of reaction energy calculation, full-scanned neural network (NN) simulation and new physical kinetics modeling. Degradation kinetics, mechanisms and activity of degradation catalyst, etc., were studied. As a result, the reaction energy calculation figured out eight potential degradation pathways of NOR with the corresponding intermediate. NN process with fully scanned parameters showed dominating advantage compared to non-linear regression and first-order law in simulation work. With the obtained database from NN, the new physical model successfully distributed degradation contribution into direct, indirect and water flow routes. The new methodology helped to gain more valuable information with less experimental work, which guided the efficient and greener investigation process in corresponding studies.

1. Introduction

Methods for organics treatment such as photo-Fenton, electro-Fenton, photocatalysis and electro-photocatalysis offer high efficiency, feasibility, automation, and energy savings in the degradation and elimination of hazardous organics [1–4]. The study of new methods is always centered on the properties of catalyst materials, where established physical, photo, electro, and computational techniques have been widely implemented. However, the investigation of treatment performances, kinetics, and mechanisms during the interaction between treatment power and organics is also essential for developing and applying these methods. In this instance, conventional investigation techniques have revealed deficiencies and flaws, such as low study efficiency, high consumption, inaccurate results, etc [5].

Firstly, innovative techniques with a new system and catalysis materials already showed high potential to reduce hazardous organic pollution in the water phase [6,7]. However, the use of removal ratio to directly indicate the degree of degradation requires further evaluation. The study of degradation mechanisms is an additional intriguing topic. The use of radical scavengers to determine functional species and their contribution percentage to degradation has been successful. However, due to the compensatory effect of other degradation-driving forces, the simple difference in performance between the presence and absence of a particular radical cannot adequately characterize its contribution. Use the kinetic coefficient k from a simple first or second order law as an indicator to solve this problem[8,9]. But in the complex environment of

* Corresponding author.
** Corresponding author at: College of Environmental Science and Engineering, Nankai University, Tianjin 300350, PR China.
E-mail addresses: zzz_nku@163.com (Z. Zhang), hongbingyu1130@sina.com (H. Yu).

https://doi.org/10.1016/j.apcatb.2022.122184
Received 28 July 2022; Received in revised form 10 October 2022; Accepted 13 November 2022
Available online 14 November 2022

environmental degradation, these laws are insufficient to portray the complete picture.

The next issue is inaccurate testing and the massive need for testing resources. On one hand, testing degradation pathways and functional free radicals always involves massive and replicated rounds. For instance, commonly applied liquid chromatography-mass spectrometer (LC-MS) and electron spin resonance (ESR) tests experience interrupt from complicated degradation intermediates and electrolytes, which may cause major error and bias [10,11]. Massive and replicated testing is always applied to gain valuable information, which causes huge consumption of resources. On the other hand, the information mining is also definitely lacking. The treatment performance lacks in-depth analysis when compared to the mature and completed techniques for identifying and evaluating catalyst materials. Although numerous models and simulations are already performed, the analysis in most cases still relies on the simple first and second reaction orders. Overall, conventional investigation techniques have demonstrated their flaws in logic, waste of resources and time, inaccuracy, and lack of data mining. The root of these problems should be solved by relying on an experimental investigation in all aspects, with limited and concise mathematical analysis [9,12]. Therefore, extensive synergistic work between experimental work and statistics is urgently required to solve this problem. Intriguingly, this research topic demonstrates profound insight.

In this study, we intend to introduce a new calculation method to aid in the experimental investigation of organic treatment processes. Therefore, simpler and fewer laboratory experiments can yield more useful data. Reaction energy calculation, full-scan NN simulation, and new physical kinetics modeling form the system's core. Consequently, grey relation analysis (GRA) and principal component analysis (PCA) are used to examine the correlation between various variables. The outcomes of the preceding processes are then synthesized and analyzed to generate new insights. As the focus of this study, norfloxacin (NOR) degradation in saline wastewater by novel electro-photo catalysis in continuous-flow mode has been chosen. With the synergistic work between the new methodology and experimental work, a wealth of exploration accomplishments and decreased lab work consumption can be anticipated.

2. Experimental section

2.1. Experiment set-up

In this study, as depicted in Fig. S1, a novel electro-photo degradation system in the continuous-flowing mode for NOR treatment in saline wastewater was developed. As double working electrodes for degradation, the economical and high-performance Ti/SnO_2-Sb anode (TSSA) and carbon black air diffusion cathode (ADC) were selected. During the reaction, the reaction utilized continuous-flow mode in a 130 mL-capacity PTFE electro-photo catalysis reactor. As target wastewater, NOR and NaCl were added to deionized water in a specific concentration. For efficient photocatalytic reduction, quartz glasses were arranged parallel to the anode and cathode, allowing radiation to be directly attracted to the electrodes' surfaces. The electro and photocatalysis were activated at the start of the experiment to begin the degradation process. The variation of total organic carbon, NOR concentration, pH, and degradation intermediates were recorded as key information. In addition, critical effect factors such as current density, initial pH value, and hydraulic retention time (HRT) were studied.

2.2. New methodology

A new methodology has been developed based on a new synergistic work of reaction energy calculation, full-scanned NN simulation, and new physical kinetics modeling. The objective is to collaborate with simple experimental testing for effective information mining, thereby enhancing new discoveries and research value, the flowchart is as shown in Scheme 1. Consequently, research on treatment processes can be made more efficient and environmentally friendly by relying less on complex and replicated testing and relying more on reasonable calculation methods.

Specifically, the reaction energy calculation aids in determining the most probable organic degradation route. A new application of NN with fully scanned parameters is conducted to simulate data based on testing in order to expand the database for further analysis. Then, based on the new database, a new physical model distributes the kinetics of corresponding reactions in great detail. After discussing the reaction mechanisms, the nature of the catalyst and electrolyte in the catalysis procedure can be determined. Using GRA and PCA analyses, correlations between variables were investigated.

2.2.1. Systematic energy calculation

A systematic calculation of the degradation process yielded crucial data regarding degradation reaction energies and potential degradation pathways. It was a significant experiment on degradation pathway compensation. In this calculation process, we considered the initial and further degradation pathways to reveal new information about the first steps of degradation reaction, which has been rarely reported. In addition, the results of the calculations can be used in conjunction with other methods to support the analysis of degradation pathways. In this case, the reaction processes between NOR and oxidant agents (•Cl and •OH) were conducted by density functional theory (DFT). Using the M06–2X function with the 6–31 +G (d, p) basis set, the geometries of the reactant, complex, transition state (TS), intermediate (IM), and the product were optimized for the reaction in an aqueous solution. Normal vibration frequencies were used to study the nature of stationary points, where all reactants, complexes, and IM must exhibit positive real frequencies. The minimum energy path (MEP) was determined using the theory of intrinsic reaction coordinates (IRC). All calculations were performed by the Gaussian 09 software. Water was considered a solvent for simulating the internal cellular and in vitro natural environments. To study the solvation effect on reactions, integral equation formulation of the polarized continuum model (IEFPCM) and the continuum solvation model was used [13–15].

Relative Gibbs free energies in solution were computed using

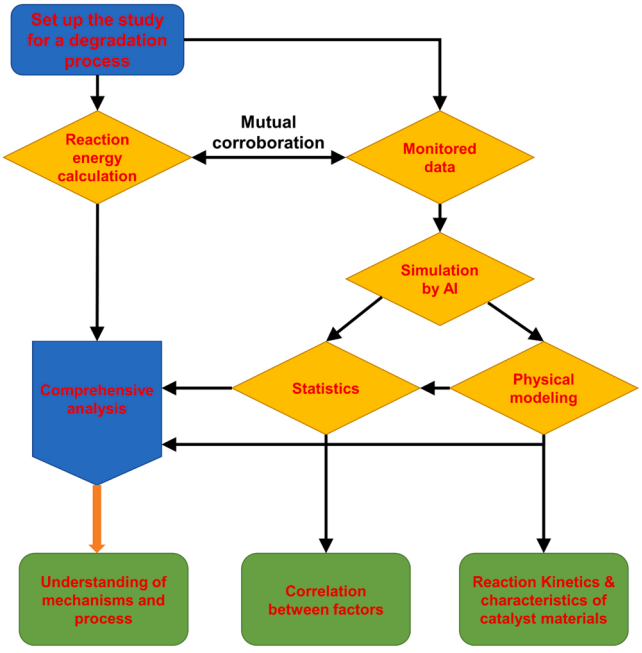

Scheme 1. The flowchart of BP-NN training process.

thermodynamic cycles and Hess law which included solvation free energies. For example, the thermodynamic cycle for the reaction of •OH with NOR is as follows:

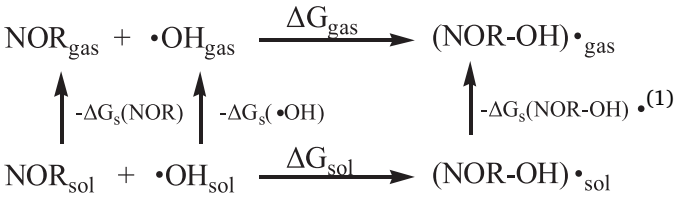

(1)

The Gibbs free energy of a reaction in solution (ΔG_{sol}) was the sum of the Gibbs free energy of a reaction in the gas phase (ΔG_{gas}) and the difference in solvation free energies ($\Delta\Delta G_s$)

$$\Delta G_{sol} = \Delta G_{gas} + \Delta\Delta G_s \quad (2)$$

The $\Delta\Delta G_s$ can be calculated as:

$$\Delta\Delta G_s = \Delta G_s(NOR - \bullet OH) - \Delta G_s(NOR) - \Delta G_s(\bullet OH) \quad (3)$$

where ΔG_s represents the solvation free energy. In all cases, the reference state is one mole.

In this work, possible initial and further degradation pathways for both abstraction and addition reactions on Norfloxacin with •OH and •Cl were selected and studied by energy calculation. The pathways which couldn't format abstraction/addition reactions in practice according to the energy calculation were excluded.

2.2.2. Modeling simulation and statistics

Important data and regulations can be condensed using this procedure for information extraction from experimental results. Noteworthily, this study implemented a new full-scanned back-propagation Neural Network (BP-NN) process for accurate simulation of experimental outputs and database enhancement [16,17]. In this instance, the weight of each nerve was not only trained but also the number of nerves in the hidden layer and the initial value during training. Therefore, superior simulation performance can be anticipated compared to simple BP-NN modeling.

The four input parameters are current density, initial pH value, hydraulic retention time (HRT), and reaction time. In that order, the three outputs included variations in TOC, NOR concentration, and pH. There was one hidden layer and one output layer. The number of nerves in the hidden layer was scanned between 5 and 20, and the training was repeated 100 times with different initial value settlements for each nerve number. The detailed parameter setting of the BP-NN training were shown in Table S1.

For comparison purposes, first-order law and multielement nonlinear regression were conducted for simulation. Because of the involvement of HRT in this study, the function of first-order law can be explained as below, taking the TOC removal ratio as an example:

$$R_t = HRT \times k \times (1 - \exp(-t/HRT)) \quad (4)$$

where R_t refers to the TOC removal ratio, with k as the reaction coefficient and t as reaction time.

Multielement non-linear regression was also carried out for simulation. As a result, the equation, considering two factors: X_1 and X_2, was as shown below:

$$R_t = a + X_1 + X_2 + X_1^2 + X_2^2 + X_1X_2 \quad (5)$$

where a is the coefficient in multielement non-linear regression.

A new kinetic modeling was conducted after the enrichment of the database by BP-NN. This model was based on a new idea of abstracting the reaction kinetic as the direct route indirect route and waterflow influence synergistic work. This method described the degradation process better than the single fixed-order laws and read more valuable information from experiment results. Meanwhile, it avoided huge errors and bias from complicated water quality models because of the reasonable complexity.

Take the TOC removal as an example; the direct mode included adsorption-degradation (Eqs. 6–7) and one-step generation of highly active free radicals (Eqs. 8–9). In this case, the reaction activity showed difficulty in accumulating with time, resulting in a relatively constant kinetic coefficient (Eq. 10):

$$MO + H_2O + hv \rightarrow \mathrm{MO}(\bullet OH) \quad (6)$$

$$\mathrm{MO}(\bullet OH) + R \rightarrow MO + CO_2 + H_2O \quad (7)$$

$$H_2O + hv \rightarrow \bullet OH + e^- + H^+ \quad (8)$$

$$O_2 + e^- \rightarrow \bullet O_2^- \quad (9)$$

$$R_r = k_1 \times C_t \quad (10)$$

where R_r is the reaction rate (mg L^{-1} min^{-1}), k_1 refers to the direct degradation coefficient with C_t representing TOC concentration at time t.

The indirect mode represents the multi-steps to format free radicals through intermediates (Eqs. 11–16). In this case, even if the terminal radicals stay unstable, the intermediates like Cl_2 and HClO accumulate reaction activity with time. A is the equivalent cumulative degradation agent in indirect mode with an accumulating rate as B (Eq. 17). In the degradation reaction with indirect mode, the coefficient k and A concentration can be integrated as total coefficient k_2 (Eq. 18).

$$2Cl^- - 2e^- \rightarrow Cl_2 \quad (11)$$

$$Cl_2 + 2OH^- \rightarrow ClO^- + Cl^- + H_2O \quad (12)$$

$$H^+ + ClO^- \rightarrow HClO \quad (13)$$

$$ClO^- + hv \rightarrow \bullet Cl + \bullet O^- \quad (14)$$

$$HClO + hv \rightarrow \bullet OH + \bullet Cl \quad (15)$$

$$Cl_2 + hv \rightarrow 2 \bullet Cl \quad (16)$$

$$DA/Dt = k_2 \quad (17)$$

$$R_r = (k_1 + k_2) \times C_t \quad (18)$$

Using this model's differential equations, a data simulation was then performed in stages. Consequently, the kinetics can be described in the direct and indirect modes, and the potential variation of coefficients k1 and k2 by reaction environment and material corrosion can also be expressed. The result of the direct simulation will be the kinetic coefficient k1 for the direct route and the equivalent agent accumulation rate B for the indirect route.

In this work, grey relation analysis (GRA) was employed as a statistical technique for data analysis. GRA was utilized to determine the degree of correlation between two or more factors. For example, the relationship was studied between operating time, TOC removal ratio, pH variation, NOR removal ratio, and rate. In the GRA analysis, each factor was chosen once as a reference for all experimental conditions. The result provided insight into the differences in degradability between experimental environments.

3. Results and discussion

3.1. Systematic calculation of degradation process

The degradation process was calculated using free radicals due to the strong guiding function of the entire NOR degradation analysis. In this

case, two main radical groups, chlorine and oxygen radicals, were represented by •Cl and •OH. In addition, as shown in Figs. S2-S5, 32 initial degradation pathways were considered driven by abstraction and addition reaction based on theoretical calculations.

3.1.1. Initial degradation pathways by •OH

Ten extraction reactions and ten addition reactions are accounted for in the calculations (Figs. S2-S3). ΔG is shown in Tables S2-S3 with the corresponding variation in reaction energy shown in Fig. 1a and b. All H-abstraction reactions in aqueous solution (Fig. S3) are exergonic (ΔG<0), indicating spontaneous occurrence [18,19]. This is consistent with identifying optimal equilibrium geometries for complexes and transition states (TSs). All formatting bonds exhibit greater stretching than existing C-H bonds, indicating that all TSs of NOR in H-abstraction reactions are reactant-like. Hammond's postulate predicts that reactions involving reactant-like TSs will be exothermic.

In contrast, the F-abstraction reaction (R5) is endergonic (ΔG>0) and thus thermodynamically impossible. In addition, the pathways R1 and R3 are barrier-free reactions. The corresponding initial reactant complexes CR1 and CR3 possess less energy than the reactant whose relative energies are depicted in Fig. 1a. Consequently, the R1 and R3 reaction pathways are more dynamically favorable. R2 is the most exergonic of all H-abstraction reactions, referring to the H abstraction from the C-H bond connected to the N-H bond on the piperazine ring [20]. Thus, the R2 reaction pathway is thermodynamically more favorable.

Most addition reactions occur on quinoline, carboxyl, and carbonyl groups, producing OH-adduct radicals (Fig. S3). According to the results of the calculations, all addition reactions are exergonic (ΔG<0) and thermodynamically feasible (Table S3 and Fig. S1b). The majority of addition reaction active sites are C═C double bonds substituted with an F atom and a carboxyl group. R12 and R19 are both barrier-free reactions, with R12 being the most exergonic [21]. This result is likely attributable to the strong electronegativity and electron absorption capacity of the F atom, which strengthens the electro-positivity of carbon atoms connected to the F atom, thereby facilitating the addition of •OH [22,23]. By analyzing the R12 process, it is discovered that the addition of •OH is accompanied by the dissociation of the F atom; this is a synergistic process. In contrast, the addition of •OH to R19 under the influence of the carboxyl group results in the formation of CR19. The opening of the C═C double bond would then occur [24].

Regarding reaction energy (Fig. 1b), the R12 and R19 pathways should be preferred. The respective IM12 and IM19 are more accessible than other IMs. Due to the stable structure of the benzene ring, its subsequent ring-opening from IM12 cannot occur prior to the addition-initiated degradation processes. Therefore, the priority of the C-N hexatomic ring opening after R19 is relatively higher.

3.1.2. Initial degradation pathways by •Cl

Fig. S4 depicts ten initial abstraction reactions, including nine H-abstraction (R1-R4, R6-R10) and one F-abstraction (R5) conditions with plotted relative reaction energy variations in Fig. 2a and b. Three H-abstraction reactions, R1, R2, and R8, are determined to be barrier-free, indicating that they are more dynamically favorable than other

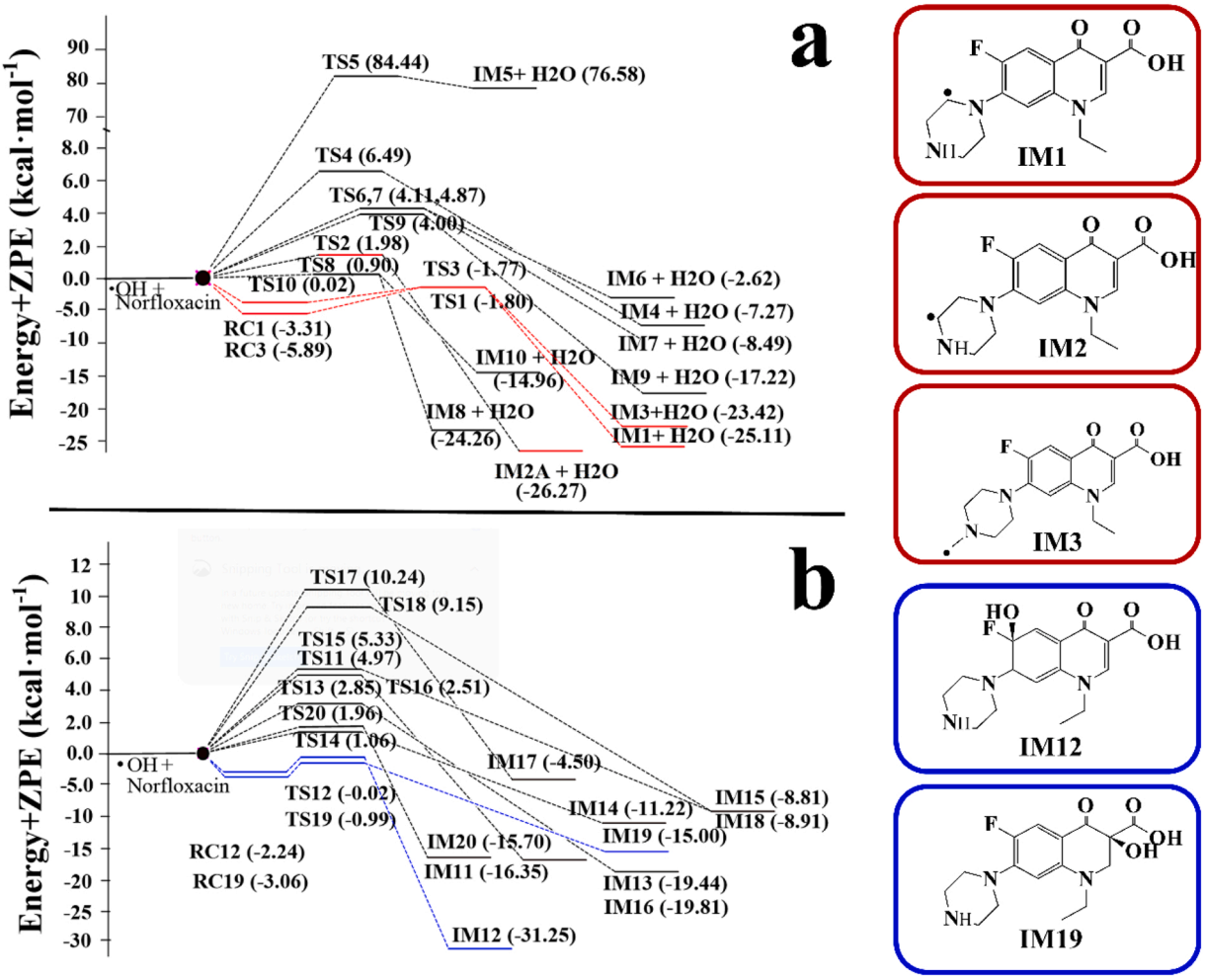

Fig. 1. The reaction energy of initial (a) abstraction and (b) addition reactions on NOR with •OH.

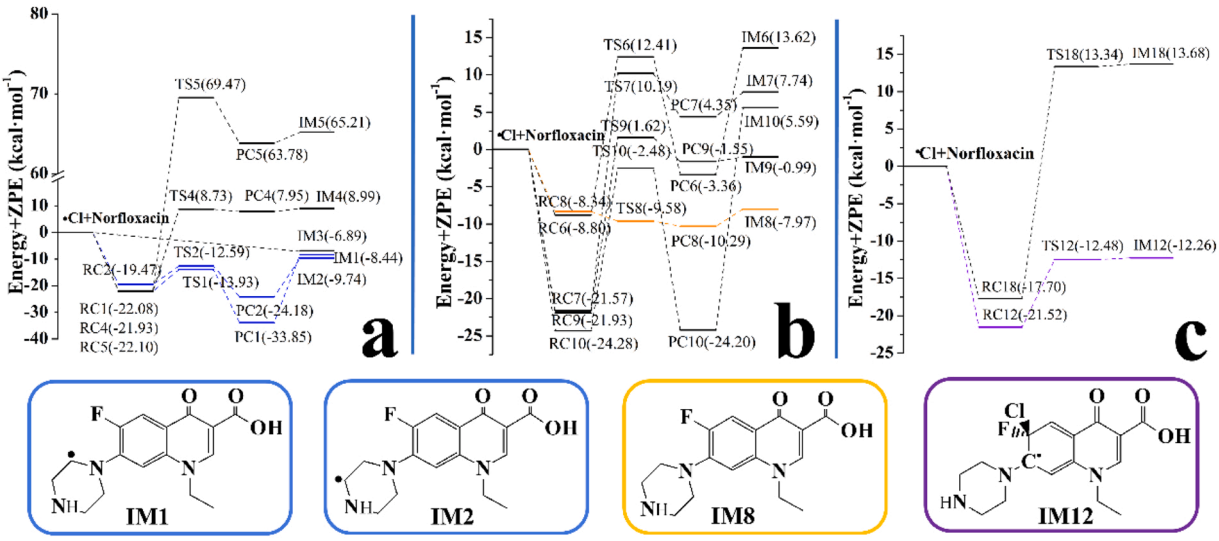

Fig. 2. The reaction energy of initial abstraction ((a)-(b)) and addition (c) reactions on NOR with •Cl.

reactions [25,26]. R2 is the most exergonic of all involved abstraction reactions, referring to the H abstraction from the C-H bond in addition to the N-H bond on the piperazine ring, which is consistent with the conclusion in •OH involved abstraction. Therefore, pathway R2 is thermodynamically more favorable than alternative abstraction reactions. Considering its barrierless condition, R2 should be the initial abstraction reaction of NOR-•Cl. In contrast, the F-abstraction reaction (R5) is endothermic. For its occurrence, a high energy barrier and high energy consumption must be overcome. Similar to the situation in •OH-driven abstractions, it is difficult for the •Cl radical to abstract the F atom.

As depicted in Fig. S5, two potential addition reaction pathways, R12 and R18, are considered between NOR and •Cl. The corresponding variations in reaction energy are depicted in Fig. 2c. On quinoline and carboxyl groups, these reactions produce OH-adduct radicals. R12 is determined to be barrierless and exergonic, making it dynamically and thermodynamically advantageous [27]. However, R18, which has a high barrier (13.3 kcal mol^{-1}) and high energy consumption (13.7 kcal mol^{-1}), should not be considered as a primer for the initial addition reaction between NOR and •Cl. In the meantime, the subsequent reactions after R12 occur on the refractory benzene ring with the lowest reaction energy, demonstrating the difficulty of their occurrence. To further investigate the degradation pathway, the reaction routes from potential abstraction reactions R1, R2, and R8 must therefore be emphasized.

3.1.3. *Further ring-open reactions*

The study of further ring-opening reaction is based on the prior initial degradation pathways, including R1, R2 and R19 by •OH and R1, R2, and R8 by •Cl. The corresponding intermediates are IM1, IM2, IM19 and IM1, IM2, and IM8 for two radicals, respectively, as shown in Fig. S6 and Fig. S7.

3.1.4. *•OH degradation route*

In the •OH degradation route in Fig. S6a, IM1 is an energy-rich radicals which can react with •OH to form IM21 in a barrierless and heat releasing. IM21 may undergo a ring-opening reaction through different pathways. The first way refers to the hydrogen transformation reaction on the hydroxy group, occurring with the ring opening between C2 and N1 (R21) and between C2 and C3 (R22). However, these pathways are determined as thermodynamically unfavorable. The other pathway goes through an H abstraction from the hydroxy group IM21 by •OH, formatting a radical IM22. This process is exothermic and barrierless association. Subsequently, the ring-opening on the piperazine ring may occur on C2-C3 (R23) and C2-N1 (R24) bond. The R23 process has a low energy barrier of 0.22 kcal mol^{-1}, while R24 needs to span the energy barrier of 9.69 kcal mol^{-1}. R23 degradation pathway is therefore considered as prior.

Similar to IM1, two ring-opening pathways are considered after transforming IM2 to IM23 by •OH in an aqueous solution, as shown in Fig. S6b. The formation of IM23 is a barrierless association and released heat of 97.1 kcal mol^{-1}. Pathways R25 and R26 refer to the ring-opening from IM23 with hydrogen transfer reaction. Due to the high energy, the two pathways and their products, P5 and P6, cannot be a primer in the ring-opening process of IM2. On the other hand, pathways R27 and R28 are derived from the radical IM24, which transforms from IM23 by the attraction of •OH. The formation of IM24 faces an energy barrier of 5.38 kcal mol^{-1}. The following R27 with C2-C3 breaking owns a low energy barrier of 2.43 kcal mol^{-1}, and the process is exothermic by 23.97 kcal mol^{-1}, showing an advantage to R28. Therefore, R27 should be considered as prior among all pathways from IM2.

IM19 would further format IM25 by a further combination with •OH. This process is a barrierless association and releases heat of 94.1 kcal mol^{-1}. The subsequent possible ring-opening ways from IM25 are described in Fig. S7. The first degradation route from IM25 refers to the direct ring-opening with hydrogen transformation. However, all corresponding sub-pathways (R29-R32) have high energy barriers and are endothermic. The second route is from the continuous reaction between IM25 and •OH, resulting in the exothermic IM26 and P15. IM26 would then undergo a ring-opening reaction on C-N hexatomic ring (R33, R34, R36). Among them, R36, formatted by breaking C6-C7 from IM26, shows higher heat release. Therefore, R36 is considered a primer degradation pathway with P16 as the main possible product of C-N hexatomic degradation from IM19.

3.1.5. *•Cl degradation route*

In the •Cl degradation route, the further ring-opening reactions initiated by abstraction reactions R1, R2 and R8 are studied with their schematic diagrams shown in Fig. S6c and d. The active radical IM1 from R1 can further react with •Cl to form M21, with a large energy release ($\Delta H^{\ominus}_{298}$ = 81.7 kcal mol^{-1}). This is due to the high reaction activity of both free radicals [26]. However, the further transformation to IM22 and IM 23 are unfavorable due to their higher energy barrier and endothermic degree. Similarly, the favorable degradation route from IM2 ends at IM24 [28].

The ring-opening from IM8 is not thermodynamically favorable.

Without the further addition by •Cl, the breaking of the N8-C8 bond performs a high variation of Gibbs free energy ($\Delta G = 57.4$ kcal mol^{-1}) and high heat adsorption (49.5 kcal mol^{-1}) to form IM26 (Fig. S6d). With the assistance of additional •Cl, the heat adsorption remains as plus ($\Delta H^{\ominus}_{298} = 45.5$ kcal mol^{-1}). Therefore, the ring-opening reaction should be considered less significant in the degradation process. Alternatively, IM21 and IM24 from pathway 22 and 23 should be primers.

Overall, in all degradation pathways by •OH and •Cl, R23, R27, R36 for •OH and R22, and R23 for •Cl are as prior, with the most favorable intermediates as P3 (Fig. S6a), P7 (Fig. S6b) P16 (Fig. S3), IM21 (Fig. S6d) and IM24 (Fig. S6d).

3.2. Degradation performances and analysis

3.2.1. Performances

The degradation performances in the function of current density (Fig. 3a-c), HRT (Fig. 3d-f) and combined current density-pH (Fig. 3g-i) are displayed. Notably, the dispersion degree of TOC and pH value in various conditions shows significance compared to that of NOR. The integral coefficient of variation for TOC and pH (0.456 and 2.12) is significantly higher than that for NOR (0.0982). This is consistent with the fast initial addition and abstract reactions confirmed in Section 3.1, leading to a rapid decrease in NOR concentration with no significant relationship to the degradation process. Consequently, the effects of time, current density, pH, and HRT on NOR value are negligible. As a

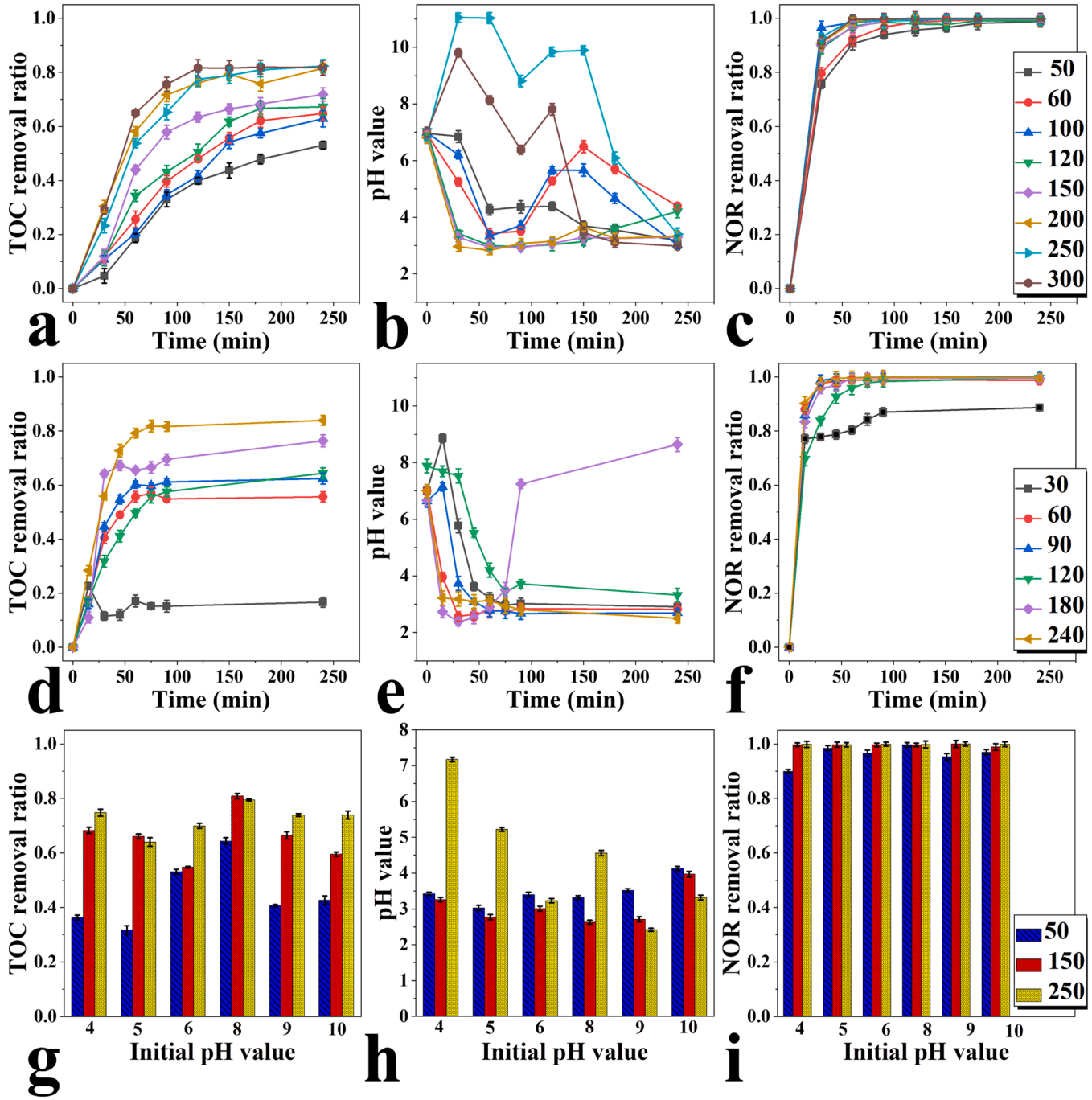

Fig. 3. The variation of TOC, pH values and NOR concentration during experiments. (a)-(c) in the function of current density, mA cm^{-2}; (d)-(f) in the function of HRT, min; (g)-(I) in the function of combined current density-pH, with 50, 150 and 250 mA cm^{-2} current density applied.

result, the NOR value is a poor indicator of the degradation process; rather, TOC and pH variation should be emphasized.

As shown in Fig. 3a, the TOC removal can be enhanced by higher current density due to the accelerated charge carrier transportation and the subsequent formation of holes and oxidant agents [29,30]. Moreover, lower HRT lift organic pollutant loading and significantly reduce the TOC removal ratio in the discharge (Fig. 3d). However, when the TOC removal ratio in all conditions reaches a stable status before 240 min of running time, the kinetic coefficient showed a more uniformity of degradation performance than the removal ratio. From 60 min, the HRT has increased fourfold to 0.0151 ~ 0.0218 min^{-1}. These indicate the limited effect on the reaction activity in the system by HRT. In the combined function of current density-pH, a pyramid-type TOC removal ratio is obtained with increasing pH value in all conditions of current densities (Fig. 3g). The neural condition of pH= 8 indicates prior degradation performances, which can be attributed to the free radical production chain inhibition in highly acid or alkaline electrolytes [31,32]. However, with increasing current density, the influencing role of pH is interrupted. The variation coefficient of the TOC removal ratio reduced from 0.267 to 0.0719 with current density from 50 to 250 mA cm^{-2}, respectively. This should be explained as a simple overlapping of the effect of pH value by increasing current density.

In terms of pH variation, the final acidic condition in most experiments (Fig. 3b, e and h) should be due to the oxidant agent production process under photo-electro catalysis (Eqs. 8 and 12). However, the clear relation between faster controlling of pH and higher current density or lower flow rate cannot be concluded (Fig. 3b and e). Regarding the combined effect of current density-pH on the pH variation (Fig. 3h), a clear lifting of final pH by higher initial pH is expressed with 50 mA cm^{-2} current density. However, this law is flipped when increased to 150 and 250 mA cm^{-2}. Therefore, the decreasing controlling role of pH to TOC removal in Fig. 3g can also be attributed to the influence of higher current density on the pH variation during the experiment.

3.2.2. Simulation

The degradation results as a function of current density, HRT, and combined current density-pH are simulated to enrich the database and speed up the subsequent exploration. Counting the experimental time, four effect factors are involved in the simulation. Tables S4-S6 depicts the simulation performance of NN, multielement non-linear regression, and first-order methods as measured by R square. Overall, the performance of simulation methods follows the order NN > regression > first order. Moreover, compared to other methods, NN exhibit greater accuracy in specific simulations and offer greater applicability for various curves as well as trends in experimental results. Considering $r^2 > 0.85$ as the standard, 89.3%, 53.6% and 100% simulations of TOC, pH and NOR remain qualified by NN, respectively. The advantage of NN derives from the continuous parameter adjustment and multi factors considered, which shows higher adaptability in complex photo-electro catalysis systems. Especially in this work, a further enhanced simulation is achieved with the further scanning of nerve numbers and initial values in the NN process.

For better observation, the concrete simulation curves are displayed in Fig. S8. Great performances of all three methods are obtained for the original data with the uniformed trend and slight radian (Fig. S8a, d and j). Oppositely, for those with complex variation and fluctuation, NN performs remarkably better in descript the detailed trend and changes in the original data (Fig. S8b, e, f, g, I, k and l). This distinguishes the performance between NN and the other two methods.

3.2.3. Degradation contribution

The degradation contribution is distributed upon the new physical kinetic modeling in this work. Direct adsorption-degradation, indirect oxidation and water flowing are three main routes of reaction kinetics, with results expressed in Fig. S9. The larger contribution by direct route is with higher current densities (1.70–17.4%) from 100 to 300 mA cm^{-2} in Fig. S9a-c, which may result from greater reaction energy supplied by the electric field. Consequently, with an uneven distribution of gaps, electrons with a larger energy gap between bands can also be excited, thereby accelerating the generation of holes for direct adsorption-degradation [27,33]. In addition, a higher current density may result in a higher ratio of redundant side reactions, which compete with chlorine evolution reaction reactions for electron supply [34]. Due to the primary role of the CER-•Cl chain in indirect degradation in salt water, the importance of the indirect route would diminish as the current density increased.

In terms of pH, the share of the direct route lifted with a higher initial pH value in the electrolyte (30.3–40.6% with pH from 5 to 10, Fig. S9d-f). This may be due to the dominating CER-•Cl chain for indirect degradation with pH ranging between 3 and 7. The higher values reduce the reaction rate, increase side reactions, and increase the direct route's contribution ratio [35,36]. However, with the pH value dropping to 3–2 during experiment in all conditions, the Cl-ClO/HClO-•Cl process remains a significant degradation contributor.

In addition, the modeling clearly illustrates the growing importance of direct routes with higher HRT (Fig. S9g-i). By increasing HRT from 90 to 240 min, the direct route's contribution rose from 24.6% to 64.0%. This is because of the lower corresponding flowrate, making it easier for the indirect route to accumulate around the catalysis interface to produce oxidants. This would prevent the production of additional oxidants and slow the diffusion of oxidants into the bulk electrolyte and subsequent mixing [37,38]. However, since there is no element of diffusion and subsequent reaction, the direct route is subject to fewer influences and performs better with a higher HRT.

The negative influence of waterflow increases with increasing current density due to a larger NOR concentration gap between inflow and outflow (Fig. S9a-c). Similar regulation also operates as a function of pH and HRT (Fig. S9d-f), where faster degradation results in a stronger waterflow interruption. Notably, according to common sense, waterflow should exert a greater influence as its velocity increases (lower HRT). However, this cannot be determined at this time (Fig. S9g-i). This is because changes in the NOR concentration gap between inflow and outflow due to varying HRT have negated the effect of flow-rate changes.

3.2.4. GRA and PCA analysis

GRA is conducted with TOC, pH, running time, NOR concentration, direct kinetic coefficient k_1 and indirect equivalent oxidant agent accumulation rate B involved. Each of them is a reference by turn. Among all factors, we select NOR concentration variation as a reference for observation (Fig. S10). This is due to its stable simple-step process following pseudo-first order, regardless of the conditions. The grey relation grade (g) of TOC increases from low to high range of current density (Fig. S10a). As the NOR concentration variation represents initial rapid addition and abstract reactions, the higher g values of TOC indicate a closer rate between initial addition and abstract reactions and subsequent ring-opening reactions with current density increased. g value of pH in Fig. S10a performs a peak area in the medium range (100–250 mA cm^{-2}), which suggests simple pH-driving reactions (for instance, Eqs. 8, 12 and 13). This is consistent with Fig. 3b, where pH curve with medium current densities follows a simple first-order trend.

In contrast, the much lower g value of pH in the low and high current density ranges (Fig. S10a) may be the result of various NOR decomposition steps. Initial pH-driving decompositions, such as H-abstraction and dicarboxylic reaction, can be prolonged by a decrease in current density and reaction power. The terminal pH-driving reactions on NOR intermediates may be imminent due to a stronger reaction with higher current density. This is also demonstrated by the two-peak pH curves in Fig. 3b, which suggest the occurrence of two pH-influencing steps during NOR degradation. Moreover, the variation of g values of pH, k1 and B with increasing initial pH is greater in the low current density mode

(Fig. S10b) than in the high current density mode (Fig. S10c), indicating that high current density covers the effect of pH variation on these factors. In the meantime, there is no discernible trend in the function of HRT (Fig. S10d).

As depicted in Fig. 4a, PCA is first conducted with the variation of current density (c). Overall, most of the variance (78–89%) can be explained in the first two components. Component 1 should correspond to a first-order variation due to its congruence with the NOR concentration. While component 2 contains integrated TOC, pH, *k*1, and B laws. Notably, when considering TOC variation as a degradation indicator, the correlation between pH and NOR degradation is significantly reduced when considering a medium current density (Fig. 4b). This demonstrates the direct dependence of pH variation on NOR decomposition at high and low current densities (Fig. 4a and c).

To determine the effect of pH on correlations, interrupt is weakened by applying a minimum current density of 50 mA cm2 (Fig. 4d-f). The first two dominant components illustrate the same laws governing the current density variation. When considering TOC and NOR as a cluster, the H^+ concentration variation in neutral conditions is more correlated to this cluster than in acidic or alkaline conditions, indicating that the NOR degradation process may have a greater influence on the pH variation when the initial pH value is neutral. This may result from the accelerated NOR decomposition in neutral electrolyte, which accelerates the release of pH-influencing intermediates [39].

Component 1 lies between a linear time flow and a logarithmic-like TOC variation in terms of the variation of HRT (Fig. 4g-i). While component 2 refers to more rapid changes exemplified by variations in H^+ concentration. A medium HRT improves the correlation between TOC, NOR, and Time compared to a low HRT due to the greater increase in the TOC removal ratio with decreasing waterflow [40]. As a result of the rapid removal of NOR, the lifting with a higher HRT is restricted regardless of the weather.

3.2.5. *Analysis of catalysis activity of material and electrolyte*

This innovative study investigates the nature of the electrode material and electrolyte's catalytic activity and electrolyte. Electrode

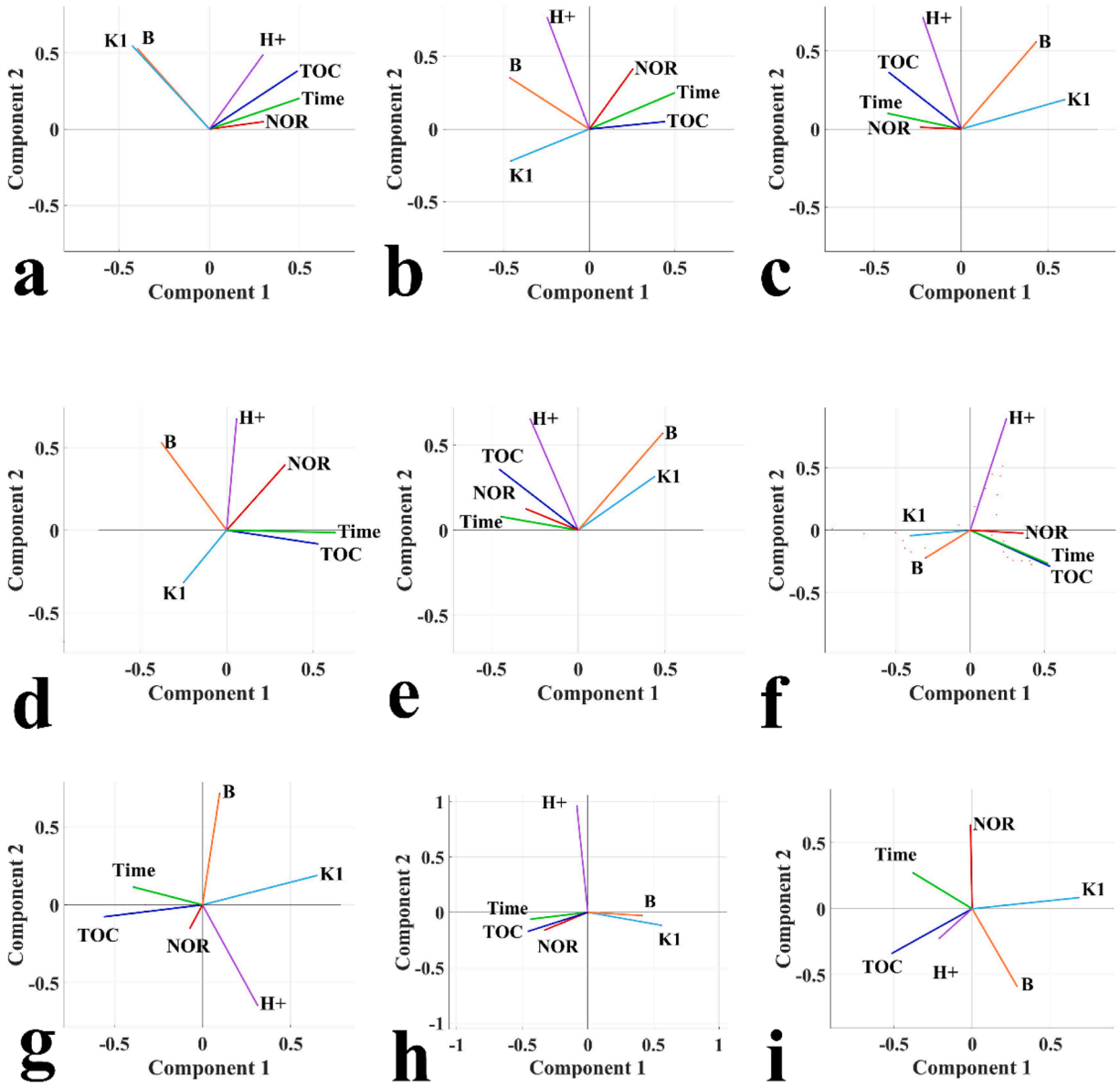

Fig. 4. Results of principal component analysis between various parameters during the experiment. (a)-(c) in the function of current density, current density= 50, 80 and 300 mA cm^{-2}, respectively; (d)-(f) in the function of initial pH, pH= 4, 6 and 10, respectively; (g)-(i) in the function of HRT, HRT= 30, 90 and 240 min, respectively.

material's catalytic activity highly depends on the energy required for electron excitation and transformation. However, the transferable electrons follow certain distributions on the required reaction energy rather than fixed energy. One example is the transition of electrons from the valence band to the conduction band. This distribution's disclosure illustrates the nature of catalysis activity. In this study, $k1$ could represent the equivalent number of excited and transferred electrons in a unit of time. The current density at the beginning of an experiment is proportional to the voltage and therefore represents the electric field strength. Its variation corresponds to the equivalent change in reaction energy for electron excitation and transformation.

Consequently, the variation of $k1$ at the beginning of an experiment as a result of lifting current density represents the equivalent electron transformation quantity per unit time as a function of the required

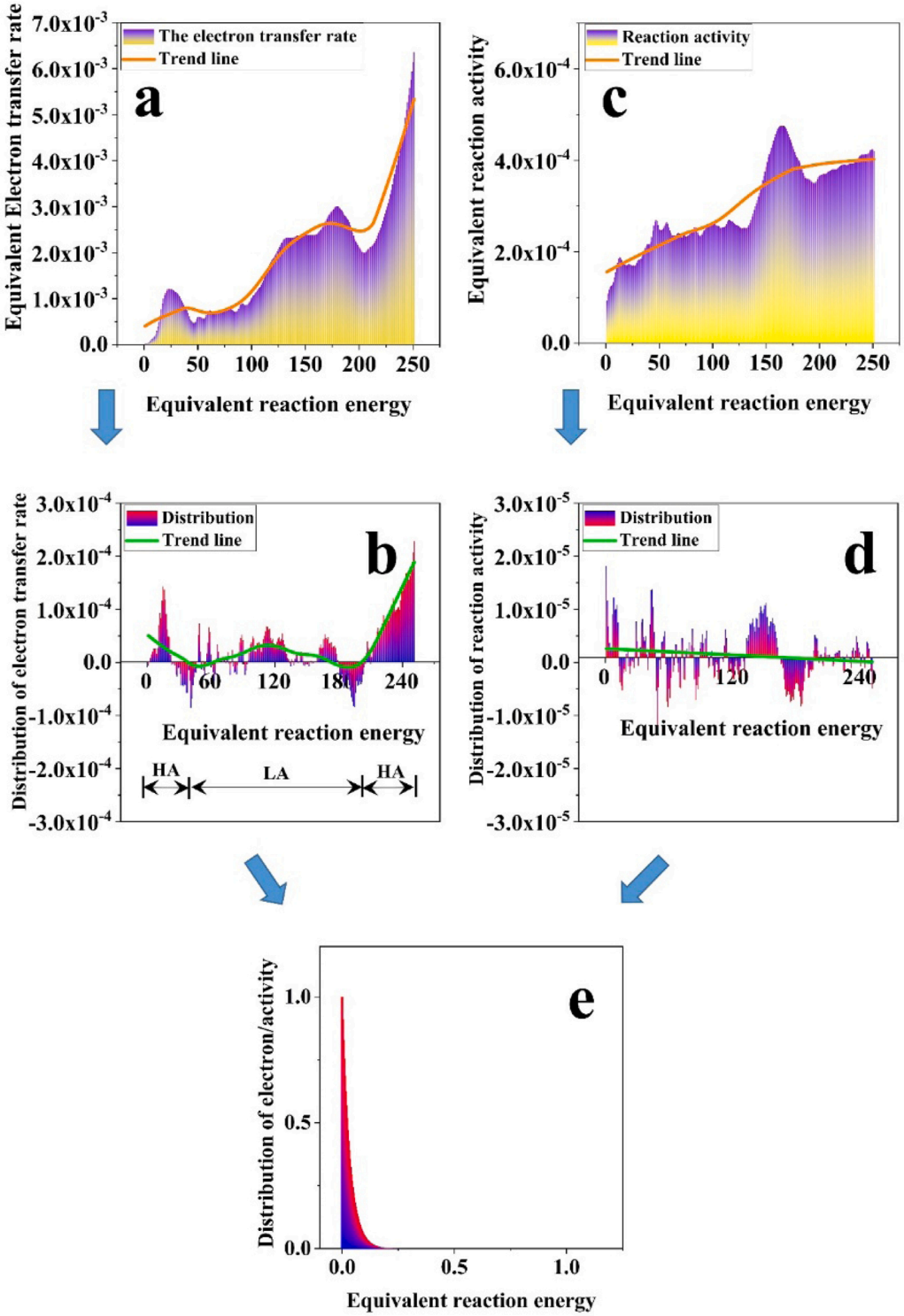

Fig. 5. The analysis of the nature of catalysis activity in electrode catalytic material and electrolyte. (a)-(b) The equivalent electron transformation rate on electrode material and its distribution on the reaction energy; (c)-(d) The equivalent reaction activity and its distribution on the reaction energy; (e) The example of the ideal distribution of both electron transformation and reaction activity.

reaction energy (Fig. 5a). Its derivative is the electron transformation distribution on the reaction energy (Fig. 5b). This work's NN simulation enables the complete scanning of current density. As shown in Fig. 5b, this distribution includes a total of 2 high-efficiency areas (HA) and 1 low-efficiency area (LA). In HA, the number of transferable electrons increases rapidly with increasing energy, whereas this number accumulates much more slowly in LA. Therefore, the HA is a region conducive to energy efficiency. Consequently, the nature of the catalytic activity of the anode of TSSA is revealed.

Similarly, B (the equivalent net oxidant agent production rate) can also be used to determine the nature of the catalytic activity of the electrode and electrolyte in combination. B refers to the indirect production of free radicals by produced agents, not the direct transformation of electrons on TSSA. However, because B represents the indirect reaction activity, it reflects the agent categories and amounts prior to their transfer to free radicals. There is a strong relationship between these and the electrolyte and electrode materials. Consequently, the total reaction activity increases as the reaction energy increases (Fig. 5c). Within the corresponding current density, the peak can be explained as the rapid fluctuation of the ratio between effective reactions (CER, oxygen reduction reaction (ORR), etc.) and invalid reactions (oxygen evolution reaction (OER), etc.).

Despite fluctuations, the distribution of reaction activity follows a general linearly decreasing trend (Fig. 5d). Slow activity accumulation should result from controlling factors such as the speed of reactant diffusion [41]. In addition, an easier free-radical production chain may hasten concentration polarization and increase the rate at which reaction activity decreases as a function of the reaction energy. The optimal distribution for transferable and reaction activity should follow the trend shown in Fig. 5e, where most transferable electrons and possible activities can be released in the low-energy region. The modeling of degradation performances can reveal the nature of the catalytic activity of the electrode material and the electrolyte. These new facets can be used to assess the properties of various catalysis materials and electrolytes for various applications.

4. Conclusion

A novel methodology to investigate the organics treatment process was successfully established and applied. A new continuous-flow photoelectro treatment of NOR was as the target subject. The methodology cooperated with simple experiments and successfully carried out valuable information in degradation kinetics, mechanisms, catalyst activities and correlations between vital variables. The concluding remarks are as below:

1. The eight most potential degradation pathways of NOR with corresponding intermediate are figured out.
2. Higher current density, hydrology retention time (HRT) and neutral environment led to prior degradation ratio (TOC removal). Whereas, NOR concentration was proven less correlated to degradation.
3. The new full scanned BP-NN process showed dominating advantage compared to non-linear regression and first-order law in simulation work of TOC, NOR and pH variations.
4. A new kinetics study distributed the degradation effect into direct, indirect and waterflow routes, where both direct and indirect routes contributed significantly to reducing the organic pollutant.
5. GRA and PCA described the correlation between parameters during the experiment, and a two-steps effect on pH value by the decomposition of NOR was suggested
6. The nature of the catalysis activity of electrode material and electrolyte was revealed by innovative utilization of obtained kinetic coefficients during modeling.

The new methodology showed a bright perspective on information mining with a simpler experimental process. Therefore, efficient investigation with less consumption during lab work can be expected. This methodology is a significant reference to investigate new organics treatment techniques and can be applied in a wide range of studies focusing on chemical processes like synthesis and decomposition in complex systems. Prior to its mature application, the methodology requires improved construction and a broader range of analysis methods, as well as the modification of additional investigation tasks.

CRediT authorship contribution statement

Han Yu: Conceptualization, Investigation, Formal analysis, Writing – review & editing, Software. **Zhenzong Zhang**: Conceptualization, Investigation, Writing – review & editing. **Sihui Zhan**: Investigation, Formal analysis. **Shuyan Song**: Investigation, Formal analysis. **Shengmin Sun:** Writing review & editing. **Hui Zhang**: Data Curation. **Linus Zhang:** Formal analysis, Writing editing. **Hongbing Yu**: Conceptualization, Funding acquisition, Formal analysis, Writing – review & editing.

Declaration of Competing Interest

The authors declare that they have no known competing financial interests or personal relationships that could have appeared to influence the work reported in this paper.

Data Availability

Data will be made available on request.

Acknowledgements

This work was supported by the National Basic Research Program of China (2016YFCO209301), Science and Technology Plans of Tianjin (21ZXCCSN00010), Shenzhen Science and Technology Program (KCXFZ20211020172542001), Tianjin Development Program for Innovation and Entrepreneurship.

Appendix A. Supporting information

Supplementary data associated with this article can be found in the online version at doi:10.1016/j.apcatb.2022.122184.

References

[1] R. Liu, Y. Xu, B. Chen, Self-assembled nano-FeO(OH)/reduced graphene oxide aerogel as a reusable catalyst for photo-fenton degradation of phenolic organics, Environ. Sci. Technol. 52 (2018) 7043–7053.
[2] Y. Zheng, J. He, S. Qiu, D. Yu, Y. Zhu, H. Pang, J. Zhang, Boosting hydrogen peroxide accumulation by a novel air-breathing gas diffusion electrode in electro-Fenton system, Appl. Catal. B:Environ. 316 (2022), 121617.
[3] Z. Zhang, Z. Pan, Y. Guo, P.K. Wong, X. Zhou, R. Bai, In-situ growth of all-solid Z-scheme heterojunction photocatalyst of $Bi_7O_9I_3$/g-C_3N_4 and high efficient degradation of antibiotic under visible light, Appl. Catal. B:Environ. 261 (2020), 118212.
[4] Z. Chi, J. Zhao, Y. Zhang, H. Yu, H. Yu, Coral-like WO_3/$BiVO_4$ photoanode constructed via morphology and facet engineering for antibiotic wastewater detoxification and hydrogen recovery, Chem. Eng. J. 428 (2022), 131817.
[5] Q. Shang, X. Liu, M. Zhang, P. Zhang, Y. Ling, G. Cui, W. Liu, X. Shi, J. Yue, B. Tang, Photocatalytic degradation of ofloxacin antibiotic wastewater using TS-1/C_3N_4 composite photocatalyst: Reaction performance optimisation and estimation of wastewater component synergistic effect by artificial neural network and genetic algorithm, Chem. Eng. J. 443 (2022), 136354.
[6] B. Liu, W. Song, H. Wu, Y. Xu, Y. Sun, Y. Yu, H. Zheng, S. Wan, Enhanced oxidative degradation of norfloxacin using peroxymonosulfate activated by oily sludge carbon-based nanoparticles $CoFe_2O_4$/OSC, Chem. Eng. J. 400 (2020), 125947.
[7] K. Wang, S. Zhan, D. Zhang, H. Sun, X. Jin, J. Wang, Three-dimensional graphene encapsulated Ag–$ZnFe_2O_4$ flower-like nanocomposites with enhanced photocatalytic degradation of enrofloxacin, RSC Adv. 11 (2021) 4723–4739.
[8] X. Zhu, Z. Wan, D.C.W. Tsang, M. He, D. Hou, Z. Su, J. Shang, Machine learning for the selection of carbon-based materials for tetracycline and sulfamethoxazole adsorption, Chem. Eng. J. 406 (2021), 126782.
[9] C. Wang, G. Mao, K. Liao, W. Ben, M. Qiao, Y. Bai, J. Qu, Machine learning approach identifies water sample source based on microbial abundance, Water Res. 199 (2021), 117185.

[10] W. Yang, Y. Wang, Enhanced electron and mass transfer flow-through cell with C_3N_4-MoS_2 supported on three-dimensional graphene photoanode for the removal of antibiotic and antibacterial potencies in ampicillin wastewater, Appl. Catal. B: Environ. 282 (2021), 119574.
[11] A. Wang, H. Wang, H. Deng, S. Wang, W. Shi, Z. Yi, R. Qiu, K. Yan, Controllable synthesis of mesoporous manganese oxide microsphere efficient for photo-Fenton-like removal of fluoroquinolone antibiotics, Appl. Catal. B:Environ. 248 (2019) 298–308.
[12] X. Xu, T. Du, D. Guo, X. Jiang, M. Zeng, N. Wu, C. Wang, Z. Zhang, Deciphering and predicting anammox-based nitrogen removal process under oxytetracycline stress via kinetic modeling and machine learning based on big data analysis, Sci. Total Environ. 796 (2021), 148980.
[13] Y. Wu, X. Zhao, S. Huang, Y. Li, X. Zhang, G. Zeng, L. Niu, Y. Ling, Y. Zhang, Facile construction of 2D g-C_3N_4 supported nanoflower-like $NaBiO_3$ with direct Z-scheme heterojunctions and insight into its photocatalytic degradation of tetracycline, J. Hazard. Mater. 414 (2021), 125547.
[14] H. Cao, M. He, D. Han, J. Li, M. Li, W. Wang, S. Yao, OH-initiated oxidation mechanisms and kinetics of 2,4,4′-tribrominated diphenyl ether, Environ. Sci. Technol. 47 (2013) 8238–8247.
[15] J. Chen, N. Wu, X. Xu, R. Qu, C. Li, X. Pan, Z. Wei, Z. Wang, Fe(VI)-mediated single-electron coupling processes for the removal of chlorophene: a combined experimental and computational study, Environ. Sci. Technol. 52 (2018) 12592–12601.
[16] S.D. Tumbo, D.G. Wagner, P.H. Heinemann, Hyperspectral–based neural network for predicting chlorophyll status in corn, Trans. ASAE 45 (2002) 825.
[17] Y.X. Hou, H.F. Zhao, Z. Zhang, K.N. Wu, A novel method for predicting cadmium concentration in rice grain using genetic algorithm and back-propagation neural network based on soil properties, Environ. Sci. Pollut. Res. 25 (2018) 35682–35692.
[18] C. Wang, S. Jia, Y. Zhang, Y. Nian, Y. Wang, Y. Han, Y. Liu, H. Ren, S. Wu, K. Yao, X. Han, Catalytic reactivity of Co_3O_4 with different facets in the hydrogen abstraction of phenol by persulfate, Appl. Catal. B:Environ. 270 (2020), 118819.
[19] C. Wang, S.-Y. Jia, Y. Han, Y. Li, Y. Liu, H.-T. Ren, S.-H. Wu, X. Han, Selective oxidation of various phenolic contaminants by activated persulfate via the hydrogen abstraction pathway, ACS EST Engg. 1 (2021) 1275–1286.
[20] J. Duan, Y. Li, J. Gao, R. Cao, E. Shang, W. Zhang, ROS-mediated photoaging pathways of nano- and micro-plastic particles under UV irradiation, Water Res. 216 (2022), 118320.
[21] X. Chen, R. Zhuan, J. Wang, Assessment of degradation characteristic and mineralization efficiency of norfloxacin by ionizing radiation combined with Fenton-like oxidation, J. Hazard. Mater. 404 (2021), 124172.
[22] Y. Jing, M. Jia, Z. Xu, W. Xiong, Z. Yang, H. Peng, J. Cao, Y. Xiang, C. Zhang, Facile synthesis of recyclable 3D gelatin aerogel decorated with MIL-88B(Fe) for activation peroxydisulfate degradation of norfloxacin, J. Hazard. Mater. 424 (2022), 127503.
[23] K. Yang, H. Lin, X. Feng, J. Jiang, J. Ma, Z. Yang, Energy-efficient removal of trace antibiotics from low-conductivity water using a Ti_4O_7 reactive electrochemical ceramic membrane: matrix effects and implications for byproduct formation, Water Res. 224 (2022), 119047.
[24] J. Guo, C. Shen, J. Sun, X. Xu, X. Li, Z. Fei, Z. Liu, X. Wen, Highly efficient activation of peroxymonosulfate by Co_3O_4/Bi_2MoO_6 p-n heterostructure composites for the degradation of norfloxacin under visible light irradiation, Sep. Purif. Technol. 259 (2021), 118109.
[25] M. Chen, W. Chu, Photocatalytic degradation and decomposition mechanism of fluoroquinolones norfloxacin over bismuth tungstate: experiment and mathematic model, Appl. Catal. B:Environ 168–169 (2015) 175–182.
[26] G. Li, S. Huang, N. Zhu, H. Yuan, D. Ge, Y. Wei, Defect-rich heterojunction photocatalyst originated from the removal of chloride ions and its degradation mechanism of norfloxacin, Chem. Eng. J. 421 (2021), 127852.
[27] J. Zhao, Z. Chi, H. Dong, C. Sun, H. Yu, H. Yu, Degradation of desphenyl chloridazon in a novel synergetic electrocatalytic system with Ni–Sb–SnO_2/Ti anode and PEDOT/PSS-CNTs modified air diffusion cathode, J. Clean. Prod. 300 (2021), 126961.
[28] Y. Lei, S. Cheng, N. Luo, X. Yang, T. An, Rate constants and mechanisms of the reactions of Cl• and $Cl_2^{\bullet-}$ with trace organic contaminants, Environ. Sci. Technol. 53 (2019) 11170–11182.
[29] S.A. Hien, C. Trellu, N. Oturan, A.S. Assémian, B.G.H. Briton, P. Drogui, K. Adouby, M.A. Oturan, Comparison of homogeneous and heterogeneous electrochemical advanced oxidation processes for treatment of textile industry wastewater, J. Hazard. Mater. 437 (2022), 129326.
[30] J. Cai, M. Zhou, Y. Pan, X. Du, X. Lu, Extremely efficient electrochemical degradation of organic pollutants with co-generation of hydroxyl and sulfate radicals on Blue-TiO_2 nanotubes anode, Appl. Catal. B:Environ. 257 (2019), 117902.
[31] L. Zhang, Y. Liu, M. Zhong, Z. Li, Y. Dong, P. Gedalanga, Insights into enhanced biodegradation of sulfadimethoxine by catalyst: Transcriptomic responses and free radical interactions, Sci. Total Environ. 774 (2021), 145641.
[32] S. Yu, R. Zhang, Y. Dang, Y. Zhou, J. Zhu, Electrochemical activation of peroxymonosulfate at Ti/La_2O_3-PbO_2 anode to enhance the degradation of typical antibiotic wastewater, Sep. Purif. Technol. 294 (2022), 121164.
[33] H. Yu, D. Dou, J. Zhao, B. Pang, L. Zhang, Z. Chi, H. Yu, The exploration of Ti/SnO2-Sb anode/air diffusion cathode/UV dual photoelectric catalytic coupling system for the biological harmless treatment of real antibiotic industrial wastewater, Chem. Eng. J. 412 (2021), 128581.
[34] T. Cui, J. Chi, J. Zhu, X. Sun, J. Lai, Z. Li, L. Wang, Tuning the size and chemisorption of FeP_4 by trace Ru doping for hydrazine-assisted hydrogen evolution in seawater at large-current-density, Appl. Catal. B:Environ. 319 (2022), 121950.
[35] M. Chen, Y. Huang, W. Chu, Exploring a broadened operating pH range for norfloxacin removal via simulated solar-light-mediated Bi_2WO_6 process, Chin. J. Catal. 40 (2019) 673–680.
[36] X. Ao, W. Wang, W. Sun, Z. Lu, C. Li, Degradation and transformation of norfloxacin in medium-pressure ultraviolet/peracetic acid process: an investigation of the role of pH, Water Res. 203 (2021), 117458.
[37] W.J. Lee, Y. Bao, X. Hu, T. Lim, Hybrid catalytic ozonation-membrane filtration process with CeO_x and MnO_x impregnated catalytic ceramic membranes for micropollutants degradation, Chem. Eng. J. 378 (2019), 121670.
[38] M. Malakootian, Y.D. Shahamat, H. Mahdizadeh, Purification of diazinon pesticide by sequencing batch moving-bed biofilm reactor after ozonation/Mg-Al layered double hydroxides pre-treated effluent, Sep. Purif. Technol. 242 (2020), 116754.
[39] Y. Yang, Z. Zhong, J. Li, H. Du, Z. Li, Efficient with low-cost removal and adsorption mechanisms of norfloxacin, ciprofloxacin and ofloxacin on modified thermal kaolin: experimental and theoretical studies, J. Hazard. Mater. 430 (2022), 128500.
[40] W. Kang, S. Chen, H. Yu, T. Xu, S. Wu, X. Wang, N. Lu, X. Quan, H. Liang, Photocatalytic ozonation of organic pollutants in wastewater using a flowing through reactor, J. Hazard. Mater. 405 (2021), 124277.
[41] L. Zhang, Y. Gao, Q. Yue, P. Zhang, Y. Wang, B. Gao, Prepartion and application of novel blast furnace dust based catalytic-ceramic-filler in electrolysis assisted catalytic micro-electrolysis system for ciprofloxacin wastewater treatment, J. Hazard. Mater. 383 (2020), 121215.